Published in final edited form as:
Lab Chip. 2011 December 7; 11(23): 3990–3998. doi:10.1039/c1lc20615j.

HIGH-SPEED, CLINICAL-SCALE MICROFLUIDIC GENERATION OF STABLE PHASE-CHANGE DROPLETS FOR GAS EMBOLOTHERAPY

David Bardin[1], **Thomas D. Martz**[2], **Paul S. Sheeran**[3], **Roger Shih**[1], **Paul A. Dayton**[3], and **Abraham P. Lee**[1,*]

[1]Department of Biomedical Engineering, University of California, Irvine, CA 92697

[2]Curriculum of Applied Sciences and Engineering – Materials Science, The University of North Carolina, Chapel Hill, NC 27599

[3]Joint Department of Biomedical Engineering, The University of North Carolina and North Carolina State University, Chapel Hill, NC 27599

Abstract

In this study we report on a microfluidic device and droplet formation regime capable of generating clinical-scale quantities of droplet emulsions suitable in size and functionality for *in vivo* therapeutics. By increasing the capillary number – based on the flow rate of the continuous outer phase – in our flow-focusing device, we examine three modes of droplet breakup: geometry-controlled, dripping, and jetting. Operation of our device in the dripping regime results in the generation of highly monodisperse liquid perfluoropentane droplets in the appropriate 3–6 μm range at rates exceeding 10^5 droplets per second. Based on experimental results relating droplet diameter and the ratio of the continuous and dispersed phase flow rates, we derive a power series equation, valid in the dripping regime, to predict droplet size by $D_d \cong 27(Q_C/Q_D)^{-5/12}$. The volatile droplets in this study are stable for weeks at room temperature yet undergo rapid liquid-to-gas phase transition, and volume expansion, above a uniform thermal activation threshold. The opportunity exists to potentiate locoregional cancer therapies such as thermal ablation and percutaneous ethanol injection using thermal or acoustic vaporization of these monodisperse phase-change droplets to intentionally occlude the vessels of a cancer.

INTRODUCTION

Embolization has emerged as an accepted modality for the treatment of various cancers, including hepatocellular carcinomas, hepatic metastases, and renal cell carcinomas.[1] The intentional occlusion of a vessel, embolization enables the reduction of blood flow into or out of that vessel, and has typically been used in cancer therapies to produce local ischemia resulting in tumor necrosis. Established methods of embolization include the placement of a metal coil or soluble gelatin sponge within the target blood vessel, or the injection of chemical or particulate agents such as ethanol or polyvinyl alcohol particles to reduce blood flow at the site of injection or immediately downstream.[1,2]

Recently the field of medical ultrasound has shown much interest in gas embolotherapy, in which acoustic or thermal energy induces a droplet emulsion with a volatile liquid core to undergo a liquid-to-gas phase transition, and volume expansion, to strategically form gas

*Corresponding Author, aplee@uci.edu, Address: 3406 Engineering Hall, University of California, Irvine, Irvine, CA 92697, Phone: (949) 824-9691, Fax: (949) 824-1727.

emboli *in vivo*, as shown in Figure 1. Acoustic droplet vaporization (ADV) specifically refers to the use of focused ultrasound to induce such a transition, in which the applied acoustic pressure supplies the necessary energy to induce superheated droplet emulsions to vaporize into microbubbles. The phase-change typically results in microbubbles five to six times larger in diameter than the original droplets, enabling these gas bubbles to occlude vessels of sufficiently small diameters, such as capillaries and some arterioles.[3,4]

Studies thus far have investigated the usefulness of ADV agents to enhance contrast in ultrasound imaging[5], to deliver therapeutics[6–8], for enhanced thermal delivery alongside high-intensity focused ultrasound (HIFU)[9], and for occlusion in animal models[10]. The choice of liquid core consists of a number of perfluorocarbons, including perfluoropentane[3,7,8,10–15], perfluorohexane[8,14], perfluorooctane[16], and perfluorobutane.[17] Encapsulation of the liquid core inside a lipid, albumin, or polymer shell reduces coalescence among the droplet population and increases the Laplace pressure sufficiently to enable these volatile emulsions to remain as superheated droplets at body temperature.[3,14]

Current methods to generate these phase-change droplets – which include sonication and high-speed mechanical agitation – typically result in a polydisperse size distribution[6,7] and a non-uniform acoustic activation threshold, as well as in droplets either too large for passage through the lung capillaries (>6 μm) or too small to occlude the desired vessel (<1 μm).[3,10] Thus required are secondary methods of size selection such as filtering[5,18] or microfluidic sorting[19] to control the sizes of these distributions. The Antoine equation predicts a negative logarithmic relationship between vaporization energy and droplet diameter[13], meaning that small droplets require more energy to vaporize than larger droplets due to increased Laplace pressure. Hence, narrowing the droplet size distribution such that it is highly monodisperse should result in a uniform response to focused acoustic pressure. As well, a monodisperse population of ADV agents may better target a specific vessel diameter to improve occlusion efficiency and efficacy, and would significantly reduce unwanted bioeffects seen *in vivo*, including delayed febrile-like reactions and respiratory distress.[10,20]

Droplet-based microfluidic systems have shown to be effective technologies to produce droplets[21,22] and microbubbles[23–25] in the micrometer diameter range with high uniformity. Yet despite the attractiveness of precision control over size, shape, and composition, these systems have traditionally been viewed as unviable as bulk manufacturing processes owing to relatively low generation rates. At present, reporting of clinical-scale generation of droplet or microbubble emulsions has been limited, and virtually absent for emulsions truly useful for *in vivo* intravenous or intra-arterial therapeutics. Most recently Castro-Hernández *et al.*[26] described a new regime for microbubble generation dependent on the formation of a strong pressure gradient at the bubble-producing region. Approximately 5 μm in diameter gas-in-water bubbles were successfully generated at the tip of a long gas ligament with rates exceeding 10^5 Hz from a single channel, though bubbles were unstable due to the lack of significant surfactant or lipid shells. Far less impressive per-channel frequencies have been observed in liquid-liquid droplet generation systems. Nisisako and Torii[27] achieved a throughput of 320 mL/h in generating approximately 100 μm droplets using a multilayer device with 256 droplet formation units, a breakup rate of 1.4×10^3 droplets per second per cross-junction. Kobayashi *et al.*[28] reported the formulation of oil-in-water emulsions at cumulative rates up to 2.2×10^4 Hz using a total of 1500 submicron-channels on single-crystal silicon plates, although the emulsions were only moderately monodisperse with a minimum coefficient of variation (CV) of 9%. In fact, frequency distributions for various liquid-liquid droplet generation systems, whether water-in-oil or oil-in-water, rarely exceed several thousand droplets per second from a single channel in forming droplets seldom smaller than 10 μm in diameter.[29] From a healthcare perspective, one could comment that there is no practical use for these aforementioned emulsions due either to insufficient

quantity or inappropriate characteristics of the emulsion. Thus, a need in microfluidics still exists for systems capable of generating clinical-scale amounts of droplet or microbubble emulsions with suitable size and functionality for therapeutics.

To overcome the limitations of past droplet generation systems, we considered the basic mechanisms of droplet generation with the intent to find a possible route to produce, in mass, micrometer-scale droplets with engineered biology. Recent publications on the physics of fluids have reported the observation of a number of distinct droplet formation modes in flow-focusing microfluidic devices.[30,31] Under controlled experimental conditions, such a device transitions from geometry-controlled mode to dripping to jetting, affecting the size and generation frequency by up to an order of magnitude. In particular, Anna *et al.*[30] allude to the dripping mode of droplet breakup as a method to yield droplets smaller than the minimum device feature size with a shorter primary breakup period than other modes, as yet demonstrated in the literature with a healthcare intent. We thus set out to use the dripping regime to meet our objective of the clinic-ready manufacture of liquid perfluoropentane droplets as phase-change agents for cancer treatment.

In this work we present a microfluidic device, operated in the dripping regime, for the super high-speed generation (>10^5 Hz) of monodisperse liquid perfluoropentane droplets in the desired size range for gas embolotherapy. Resulting droplet populations exhibit polydispersity index values of <5%, are stable at room temperature for several weeks, and are thermally vaporized at 88°C in a water bath. These liquid perfluoropentane droplets thus exhibit phase-change and are ideal for targeted vessel occlusion alongside such cancer therapies as HIFU, radiofrequency ablation (RFA), laser ablation (LA), laser-induced thermotherapy (LITT), and chemotherapy. Our microfluidic device, shown in Figure 2, features a hydrodynamic flow-focusing region and expanding nozzle geometry to generate monodisperse liquid perfluoropentane droplets encapsulated in a lipid shell.

MATERIALS AND METHODS

Device Design

The microfluidic device, made of polydimethylsiloxane (PDMS) on a glass substrate, consists of fixed geometric channels designed to direct liquid perfluoropentane and a lipid solution to an orifice 7 μm in width. Filter channels of the same dimension immediately follow both inlets to prevent clogging at the orifice. Serpentine distribution channels increase the resistance between inlets and the orifice chamber, minimizing the susceptibility of droplet generation to disruptions in the fluid flows and increasing the pressure drop along the longitudinal axis of the device. Liquid perfluoropentane and lipid distribution channels each measure 38 μm in width. The post-orifice channel measures 30 μm in width.

Device Operation: Droplet Formation Regimes

The principle behind a microfluidic flow-focusing system is to force a central stream of a dispersed phase and two side sheath flows of a continuous phase through a small orifice, causing a focusing effect and a breaking of the thread at the orifice into uniform emulsions.[32]

Most traditional flow-focusing devices have been operated in the geometry-controlled mode, termed for the large dependence of droplet size on the smallest feature size in the device – the orifice. In this mode droplets break off from the dispersed phase finger following a protrude-and-retract mechanism.[33] Droplets in the geometry-controlled mode are highly monodisperse but limited in minimum size by the width of the orifice.

An increase in the capillary number $Ca = \eta V/\gamma_{EQ}$, where η is the viscosity and V is the superficial velocity of the continuous outer phase, and γ_{EQ} is the equilibrium surface tension between the two fluid phases, leads to droplet generation in the dripping regime.[30] This regime produces monodisperse droplets smaller than the size of the orifice due to a narrowing of the dispersed phase finger. The dripping mode is characterized by a dispersed phase tip that does not retract but rather remains at a fixed location in the orifice, generating a stream of droplets off the tip due to Rayleigh capillary instability.

A further increase in the capillary number leads to droplet generation in the jetting mode, wherein the dispersed phase finger extends far into the post-orifice channel. Droplets, which break off the tip of the dispersed phase finger due again to Rayleigh capillary instability, tend to be as large or larger than the orifice width in the jetting mode and may be polydisperse.[30]

By adjusting the flow parameters and continuous phase viscosity, we thus aimed to operate our flow-focusing microfluidic device in the dripping regime to attain droplets of the desired size for gas embolotherapy (1–6 μm in diameter).

Microfabrication and Assembly

Standard soft lithography techniques[34] were used to fabricate the microfluidic devices. Devices were designed as vector-based fluidic channel geometries in Illustrator (Adobe) and printed at 20,000 DPI by CAD/Art Services. In a class 10,000 clean room, a 25 μm layer of UV-curable epoxy (SU8-25, MicroChem) was spun onto a 3-inch silicon wafer and exposed to UV-light through the photomask and developed.

Next, PDMS (Sylguard 184, Dow Corning), consisting of 10:1 prepolymer to curing agent, was poured over the patterned silicon wafer in a Petri dish to mold a silicon elastomer replica. The Petri dish was then vacuumed for at least half an hour to degas the PDMS and left overnight in a 70°C temperature-controlled dry oven to cure fully. The device was peeled from the hard master in a laminar flow chamber and inlets and outlet were punched using a blunt 18G needle. A soda lime glass slide was cleaned with isopropyl alcohol prior to use as the substrate. The cured PDMS device and clean glass slide were bonded after 150 seconds in air plasma at 250 millitorr. DI water was added to the outlet after plasma preparation and allowed to wick in order to maintain the hydrophilicity of the channels.

Chemicals

A lipid shell was chosen over an albumin shell, as albumin shells have shown an increased tendency to become lodged in the pulmonary capillaries.[10] Adapted from Hettiarachchi *et al.*[35], the lipid flow stream consists of an aqueous glycerol mixture with the stabilizing lipids DSPC (1,2-distearoyl-*sn*-glycero-3-phosphocholine, Avanti Polar Lipids) and DSPE-PEG2000 (1,2-distearoyl-*sn*-glycero-3-phosphoethanolamine-N-[methoxy(polyethylene glycol)-2000], Avanti Polar Lipids). Briefly, 5 mg DSPC and 1.96 mg DSPE-PEG2000 were combined in a glass vial and dissolved in chloroform ($CHCl_3$, Sigma) to form a homogeneous mixture. The solvent was evaporated with a nitrogen stream and the vial was placed in a vacuum chamber for a half hour to ensure a complete dry. Five mL of ultra-pure water was added to the dry lipid mixture and sonicated at room temperature for 20 minutes. The solution was combined with an additional 1 mL of ultra-pure water, 4 mL of glycerol (Sigma), and 1 mL of nonionic surfactant (Pluronic F-68, Sigma), sonicated at room temperature for 10 minutes, and stirred overnight to ensure air saturation. The lipid solution was sonicated again for 15 minutes immediately prior to use to minimize unwanted liposome formation.

Perfluoropentane (dodecafluoropentane, C_5F_{12}, FluoroMed) was chosen as the liquid perfluorocarbon. Typical physical characteristics of perfluoropentane include a boiling point of 29°C – below body temperature, 37°C – and a molecular weight of 288 g/g-mole.

Imaging and Characterization

The microfluidic device was mounted on an inverted microscope (IX71, Olympus) and external fluidic connections were made. The continuous lipid phase was supplied to the device via flexible tubing (Tygon, Sigma) and pumped at a volumetric flow rate of Q_L using a digitally controlled syringe pump (Pico Plus, Harvard Apparatus). The dispersed liquid perfluoropentane phase was delivered into the inlet of the microfluidic chamber using a homemade pressure pumping system controlled by an analytic regulator. Pressure pumping of the dispersed phase effectively minimized fluctuations in the liquid perfluoropentane flow and eliminated the buildup of pressure, characteristic of constant flow rate mechanical pumping, in the inner phase channels. As well, loading the liquid perfluoropentane was made easier by the homemade pressure pump as the low kinematic viscosity of this perfluorocarbon at room temperature (0.4 cSt) tends to complicate the loading of the syringe for mechanical pumping. The volumetric flow rate (μL/min) of the dispersed liquid perfluoropentane phase was determined from the droplet diameter D and the droplet generation frequency f_d as $Q_P = (\pi D^3/6)\, f_d * C$, where C represents the necessary conversion factors. The 30-PSI limit of the analytical regulator prevented the use of pressure pumping for the continuous lipid phase.

A high-speed camera (V310 Phantom, Vision Research) was used to record videos of the droplet generation. The image analysis program ImageJ (NIH) was used for data processing and measurements. Production rates (droplets per second) were calculated from the videos by counting the number of droplets per 500 frames and multiplying by the frame rate. Droplet diameters were back calculated from area measurements of at least 50 droplets taken optically from recorded images using ImageJ. The polydispersity index $\sigma = \delta/D * 100\%$ for each flow condition was calculated from the average droplet diameter D and standard deviation δ.

Droplet Stability

Droplets were collected in the outlet well of the microfluidic device and transferred to a sealed 7 mL glass vial. In contrast to previous reports, which stored droplets at 4–5°C[10,15], droplets in this study were stored at room temperature to assess the viability of the droplets in an on-the-shelf setting. At Days 0 and 14, 300 μL aliquots of droplet solution were pipetted onto glass slides for stability studies. ImageJ was used to analyze at least 1000 droplets, imaged in population at 40× magnification, to establish average diameter and monodispersity over the two-week period.

Vaporization of Droplets in a Water Bath

To determine the vaporization temperature of the perfluoropentane droplets, 300 μL aliquots of droplet solution were added to 2 mL of dilute lipid solution in a 7 mL vented glass vial. The elevated density of liquid perfluoropentane (1.66 g/mL) relative to the solution meant that the droplets rested at the base of the vial. The vial was suspended in a stirred water bath and the bath temperature was gradually raised until we observed gas bubble formation and thus phase transition. The experiment was conducted twice again with pure liquid perfluoropentane and pure lipid solution as controls against unintended microbubble formation.

RESULTS AND DISCUSSION

Design Optimization

Channel geometry, in addition to the compositions of fluid layers and the presence of surfactants, affects the stability of droplets post-production in the microfluidic device. Geometric optimization of the flow-focusing region enabled droplets to be produced in a single file, even at rates exceeding 10^5 Hz. To increase the distance between generated droplets at higher lipid and liquid perfluoropentane flow rates, the expanding nozzle and post-orifice channels were narrowed to widths of 70 μm and 30 μm. This narrowing minimized contact inhibitions in the high-flow velocity environment of the expansion chamber, where shell resistances are low, preventing droplet fusion before collection in the outlet well.

Droplet Formation Regimes

By adjusting the flow parameters in our flow-focusing device, we observed each of the three distinct droplet formation regimes detailed. At low continuous phase flow rates Q_L, and correspondingly low dispersed phase pressures P_P, our device produced droplets in the geometry-controlled mode. As shown in Figure 3a – comprising a series of overlaid images, successive in time – the dispersed phase finger, initially upstream of the orifice in this mode, protrudes beyond the constriction of the orifice and experiences a pinching from the sidewalls, causing droplets to shear off. This protrude-and-retract mechanism limits the droplet diameter to the width of the orifice. Droplets generated in the geometry-controlled mode ranged in diameter from 7.9 ± .1 μm at 2.44×10^4 Hz to 10.8 ± .2 μm at 3.28×10^4 Hz.

Increasing the continuous phase flow (and, correspondingly, the capillary number) causes an abrupt transition to the dripping regime of droplet formation, characterized by a dispersed phase finger that narrows to a fine tip and remains in the orifice (Figure 3b). Droplets, which break off the tip at high frequency due to “steady” Rayleigh capillary instability, vary in size according to the width of the dispersed phase finger rather than that of the orifice. Diameters of droplets generated in the dripping regime ranged from 3.6 ± .2 μm at 1.36×10^5 Hz to 10.8 ± .1 μm at 5.00×10^4 Hz.

High continuous phase flows paired with correspondingly high dispersed phase pressures transitioned droplet formation into the jetting mode. Figure 3c overlays a series of images, successive in time, to demonstrate the break off of droplets in this mode due to “dynamic” Rayleigh capillary instability; relative to in the dripping regime, the dispersed phase tip extends far beyond the orifice and fluctuates in both length and width. Droplets at the transition to the jetting regime ranged in diameter from 9.3 ± .2 μm at 7.68×10^4 Hz to 13.5 ± .1 μm at 3.84×10^4 Hz.

Generation of Liquid Perfluoropentane Droplets

The flow rate parameters are determinants for stable production and precise control over the size and generation frequency of the liquid perfluoropentane droplets. In general and regardless of the droplet formation regime, droplet diameter D – and consequently volume V – increases with the dispersed phase pressure P_P for a fixed continuous phase flow Q_L, consistent with previous studies.[23,26,35] Shown in Figure 4a, the width of the orifice limits the minimum droplet size in the geometry-controlled mode, while much smaller droplets can be generated in the dripping regime. The minimum droplet diameter tends to decrease with increasing Q_L, and thus increasing capillary number, as the smallest droplets observed in this study occurred at the highest continuous flow rates.

An interesting observation emerged when establishing trends in the droplet generation frequency f_d (Figure 4b). In geometry-controlled mode, f_d tends to increase with P_P for a fixed Q_L in order to conserve mass. Conversely, for a given Q_L in the dripping regime, decreasing P_P significantly quickens the generation frequency (increases f_d) while reducing D, hence achieving the desired super high-speed generation of functional droplets suitable for therapeutic applications. Overall and as expected, f_d tends to increase with Q_L.

The sequence of high-speed images in Figure 5 illustrates the general trends observed in the dripping regime. In particular as droplets become small, the width of the dispersed phase finger heavily influences the diameter of the droplet after it breaks off from the tip.

Shown in Figure 6 are droplet generation frequencies obtained from high-speed videos of production and corresponding polydispersity indexes, plotted as a function of droplet diameter. When operated in the dripping regime our device clearly produces liquid perfluoropentane droplets in the desired 3–6 μm range with high monodispersity at rates equal to or exceeding 10^5 Hz. Whereas no general trend appears to connect droplet diameter and generation frequency in geometry-controlled mode, D tends to decrease as f_d quickens in the dripping regime. Simple adjustment of the flow parameters enabled the generation of droplets spanning a wide range of diameters, with a polydispersity index less than 5% for each condition.

Determining the liquid perfluoropentane volumetric flow rate Q_P as detailed, we evaluated the influence of the dimensionless flow rate ratio $\varphi = Q_L/Q_P$ on droplet diameter and generation frequency. Shown in Figure 7a, a key relationship emerges in the dripping regime relating D and φ to predict droplet diameter based solely on the dimensionless flow rate ratio as $D = 27.445\varphi^{-.414}$ ($r^2 = .99$). Rounding, we characterize our flow-focusing droplet generator, operated in the dripping regime, in generic terms by

$$D_d \cong 27(Q_C/Q_D)^{-5/12} \quad (1)$$

where D_d represents the droplet diameter, and Q_C and Q_D represent the continuous and dispersed phase flow rates. Note that the exponent 5/12 matches the exponent reported in Castro-Hernández *et al.*[26] to calculate gas bubble diameter based on the ratio of the flows in a high-speed regime.

The droplet generation frequency shows relatively less dependence on the dimensionless flow rate ratio (Figure 7b). In general, however, f_d increases with φ in the dripping regime and decreases with φ in geometry-controlled mode. As in Anna *et al.*[30], transitions between the droplet formation regimes are weakly dependent on φ; rather, capillary number plays a more determining role in controlling the mode of droplet breakup.

This study used low lipid flow rates (12–26 μL/min) and correspondingly low liquid perfluoropentane pressures in order to conserve fluids and better demonstrate the viability of high-speed droplet generation as a bulk manufacturing process. By comparison, Hettiarachchi *et al.*[23] supplied the lipid phase at rates between 30–120 μL/min. Based on the trends observed in Figures 4b and 7b, even quicker droplet generation frequencies may be attained by increasing the continuous phase flow to further push the capillary number. As well, multiplexing numerous flow-focusing circuits to expand the number of droplet formation units, while maintaining device operation in the dripping regime, would scale the throughput. A 10× scale-up, for instance, would reduce the time to produce 1×10^9 droplets – similar in scale to the amount of droplets formed by mechanical agitation, and well beyond the estimated 2×10^7 monodisperse emulsions[35] necessary for therapeutics in humans – from several hours to mere minutes.

Stability

We assessed a population of droplets with a mean diameter of 4.5 μm for size stability over a two-week time span. To our knowledge this study is the first to simulate an on-the-shelf environment by storing phase-change droplets at room temperature. Over two weeks the mean droplet diameter drifted less than 4%, from 4.5 ± .2 μm to 4.3 ± .3 μm (Figure 8). It may be possible to prolong the shelf life beyond several weeks by modifying the poloxamer or PEG group, though unnecessary in practice considering that clinical phase-change and contrast agents formed via mechanical agitation are injected immediately into the patient.

Thermal Vaporization

The relatively low boiling point of liquid perfluoropentane (29°C) suggests spontaneous liquid-to-gas transition at body temperature; however, consistent with previous studies[3,14], encapsulation of the perfluorocarbon in a lipid shell increases the Laplace pressure sufficiently to stabilize the droplets well beyond the natural boiling point of pure liquid perfluoropentane. We observed rapid thermal vaporization of multiple droplet populations, collected at different days, at 88°C in a stirred water bath. Droplets remain in a superheated state prior to this activation threshold.

Shown in Figure 9, gas bubbles formed by vaporization expanded well beyond the volume predicted by the ideal gas law, $PV = nRT$, which approximates a volume expansion factor of 125[3]. Upon activation, 4.5 ± .2 μm droplets initially converted into gas bubbles 106.7 ± 4.6 μm in diameter, a diameter expansion of 24x. Kripfgans *et al.*[3] detailed this further expansion as due to the intake of dissolved gases from the host fluid after conversion of the droplet to the gas bubble of pure perfluoropentane, an effect we have observed experimentally in our previous studies with perfluorocarbons.[17] That the carrier fluid was not degassed prior to heating contributed to this large initial increase in size. Subsequent dissolution of these extra gases resulted in gas bubbles with a resting diameter of 27.4 ± 1.2 μm, a 6x increase from the original droplet diameter, imaged several days after vaporization (Figure 9, inset).

These experiments were repeated for vials containing pure liquid perfluoropentane and pure lipid solution. Under observation, pure liquid perfluoropentane transitioned directly to gas perfluoropentane, thus leaving an “empty” vial. Pure lipid solution boiled up to 120°C without the formation of gas bubbles.

The size stability of our droplets enabled consistent thermal activation of droplet populations stored at room temperature over two weeks. At threshold, droplet activation occurs in a near simultaneous manner. Likewise, we demonstrate in a parallel study that monodisperse droplets generated by our microfluidic device respond uniformly to acoustic pressure delivered from a 5 MHz piston transducer.[36] This parallel study confirms our initial hypothesis that acoustic droplet vaporization can be made homogenous by the precision engineering of phase-change agents using microfluidics.

Consistent thermal and acoustic responses make these liquid perfluoropentane droplets ideal for targeted vessel occlusion to enhance HIFU, RFA, LA, and LITT in the treatment of cancers such as hepatocellular carcinomas, hepatic metastases, and renal cell carcinomas. The inclusion of an anti-cancer drug layer within the droplet may further potentiate these treatment modalities. Our device design lends itself to the inclusion of such a drug layer by combining a second hydrodynamic flow-focusing region at the droplet formation unit, as done in microbubble studies by Hettiarachchi *et al.*[35] Chemoembolization – the addition of a chemotherapeutic agent – has been used to reduce perfusion and deliver therapeutics to treat renal cell carcinoma alongside RFA[37] and hepatocellular carcinoma alongside RFA[38] and HIFU[39]. Besides forming polydisperse size distributions, conventional production

techniques result in inconsistent drug dosages. Manufacturing utilizing microfluidics enables the accurate control of therapeutic payloads[35], and thus may improve localized drug delivery as well as thermal and acoustic responses. Further, adaptation of our microfluidic device to produce monodisperse double emulsions may enable the encapsulation of hydrophilic drugs such as thrombin[8] to extend the duration of occlusions generated by phase-change agents.

CONCLUSION

With microfluidics we can generate highly monodisperse phase-change droplets in the size range suitable for gas embolotherapy as a cancer treatment. By adjusting the flow rate of the continuous outer phase, we varied the capillary number and observed three distinct droplet formation regimes: traditional geometry-controlled mode, characterized by a protrude-and-retract mechanism of droplet break off; dripping, characterized by “steady” Rayleigh capillary instability; and jetting, characterized by “dynamic” Rayleigh capillary instability. Geometric optimization of the flow-focusing region and operation of the device in the dripping regime enabled the single-file generation of droplets at rates exceeding 10^5 Hz. To our knowledge this study is the first to report on the generation of clinical-scale quantities of droplet emulsions truly suitable for *in vivo* intravenous therapeutics.

For our flow-focusing device operated in the dripping regime, we can predict droplet diameter D_d based on the dimensionless ratio of the flow rates of the continuous outer phase Q_C and the dispersed inner phase Q_D. In simplified terms, we characterize our device in the dripping regime by $D_d \cong 27(Q_C/Q_D)^{-5/12}$.

Droplet populations generated by our microfluidic device are monodisperse, stable at room temperature, and transition uniformly to gas bubbles when presented with thermal and acoustic stimuli. Looking ahead, we aim to build a drug layer into our liquid perfluoropentane droplets to generate, using super high-speed microfluidics, phase-change droplets for gas chemoembolotherapy. Simultaneous delivery of a chemotherapeutic agent should elevate local concentrations of the drug with little escape to the systemic circulation due to vessel occlusion. Combining gas chemoembolotherapy with locoregional therapies such as thermal ablation and percutaneous ethanol injection presents a nice prospect to enhance heat and alcohol trapping and more effectively treat cancers.

Acknowledgments

The authors would like to thank Andrew Hatch and Robert Lin of our BioMiNT lab UC Irvine for discussions regarding this project. The National Institutes of Health, Grant #1 RO1 EB008733-01A1, provided funding for this work.

REFERENCES

1. Goode JA, Matson MB. Embolisation of cancer: What is the evidence? Cancer Imaging. 2004; 4:133–141. [PubMed: 18250022]
2. Kalman D, Varenhorst E. The role of arterial embolization in renal cell carcinoma. Scandinavian Journal of Urology and Nephrology. 1999; 33(3):162–170. [PubMed: 10452291]
3. Kripfgans OD, Fowlkes JB, Miller DL, Eldevik OP, Carson PL. Acoustic droplet vaporization for therapeutic and diagnostic applications. Ultrasound Med. Biol. 2000; 26(7):1177–1189. [PubMed: 11053753]
4. Apfel, RE. Activatable infusible dispersions containing drops of a superheated liquid for methods of therapy and diagnosis. United States: Apfel Enterprises, Inc.; 1998. Kripfgans 2002, In vivo droplet vaporization for occlusion therapy and phase aberration correction

5. Kripfgans OD, Fowlkes JB, Woydt M, Eldevik OP, Carson PL. *In vivo* droplet vaporization for occlusion therapy and phase aberration correction. IEEE Transactions on Ultrasonics, Ferroelectrics, and Frequency Control. 2002; 49(6):726–738.
6. Rapoport N, Chistensen DA, Kennedy AM, Nam K-H. Cavitation properties of block copolymer stabilized phase-shift nanoemulsions used as drug carriers. Ultrasound Med. Biol. 2010; 36(3):419–429. [PubMed: 20133040]
7. Fabiilli ML, Haworth KJ, Sebastian IE, Kripfgans OD, Carson PL, Fowlkes JB. Delivery of chlorambucil using an acoustically-triggered perfluoropentane emulsion. Ultrasound Med. Biol. 2010; 36(8):1364–1375. [PubMed: 20691925]
8. Fabiilli ML, Lee JA, Kripfgans OD, Carson PL, Fowlkes JB. Delivery of water-soluble drugs using acoustically triggered perfluorocarbon double emulsions. Pharm. Res. 2010; 27:2753–2765. [PubMed: 20872050]
9. Zhang P, Porter T. An *in vitro* study of a phase-shift nanoemulsion: A potential nucleation agent for bubble-enhanced HIFU tumor ablation. Ultrasound Med. Biol. 2010; 36(11):1856–1866. [PubMed: 20888685]
10. Zhang M, Fabiilli ML, Haworth KJ, Fowlkes JB, Kripfgans OD, Roberts WW, Ives KA, Carson PL. Initial investigation of acoustic droplet vaporization for occlusion in a canine kidney. Ultrasound Med. Biol. 2010; 36(10):1691–1703. [PubMed: 20800939]
11. Kripfgans OD, Fabiilli ML, Carson PL, Fowlkes JB. On the acoustic vaporization of micrometer-sized droplets. J. Acoust. Soc. Am. 2004; 116(1):272–281. [PubMed: 15295987]
12. Lo AH, Kripfgans OD, Carson PL, Rothman ED, Fowlkes JB. Acoustic droplet vaporization threshold: Effects of pulse duration and contrast agent. IEEE Transactions on Ultrasonics, Ferroelectrics, and Frequency Control. 2007; 54(5):933–946.
13. Rapoport NY, Kennedy AM, Shea JE, Scaife CL, Nam K-H. Controlled and targeted tumor chemotherapy by ultrasound-activated nanoemulsions/microbubbles. J. Controlled Release. 2009; 138:268–276.
14. Gieseke T, Hynynen K. Ultrasound-mediated cavitation thresholds of liquid perfluorocarbon droplets *in vitro* . Ultrasound Med. Biol. 2003; 29(9):1359–1365. [PubMed: 14553814]
15. Schad KC, Hynynen K. *In vitro* characterization of perfluorocarbon droplets for focused ultrasound therapy. Phys. Med. Biol. 2010; 55:4933–4947. [PubMed: 20693614]
16. Fabiilli ML, Haworth KJ, Fakhri NH, Kripfgans OD, Carson PL, Fowlkes JB. The role of inertial cavitation in acoustic droplet vaporization. IEEE Transactions on Ultrasonics, Ferroelectrics, and Frequency Control. 2009; 56(5):1006–1017.
17. Sheeran PS, Wong VP, Luois S, McFarland RJ, Ross WD, Feingold S, Matsunaga TO, Dayton PA. Decafluorobutane as a phase-change contrast agent for low-energy extravascular ultrasounic imaging. Ultrasound Med. Biol. 2011; 37(9):1518–1530. [PubMed: 21775049]
18. Lo AH, Kripfgans OD, Carson PL, Fowlkes JB. Spatial control of gas bubbles and their effects on acoustic fields. Ultrasound Med. Biol. 2006; 32(1):95–106. [PubMed: 16364801]
19. Huh D, Bahng JH, Ling Y, Wei H-H, Kripfgans OD, Fowlkes JB, Grotberg JB, Takayama S. Gravity-driven microfluidic sorting device with hydrodynamic separation amplification. Anal. Chem. 2007; 79(4):1369–1376. [PubMed: 17297936]
20. Kripfgans OD, Orifici CM, Carson PL, Ives KA, Eldevik OP, Fowlkes JB. Acoustic droplet vaporization for temporal and spatial control of tissue occlusion: A kidney study. IEEE Transactions on Ultrasonics, Ferroelectrics, and Frequency Control. 2005; 52(7):1101–1110.
21. Tan Y-C, Fisher JS, Lee AI, Cristini V, Lee AP. Design of microfluidic channel geometries for the control of droplet volume, chemical concentration, and sorting. Lab Chip. 2004; 4:292–298. [PubMed: 15269794]
22. Nisisako T, Torii T, Higuchi T. Droplet formation in a microchannel network. Lab Chip. 2002; 2:24–26. [PubMed: 15100856]
23. Hettiarachchi K, Talu E, Longo ML, Dayton PA, Lee AP. On-chip generation of microbubbles as a practical technology for manufacturing contrast agents for ultrasonic imaging. Lab Chip. 2007; 7:463–468. [PubMed: 17389962]

24. Talu E, Hettiarachchi K, Zhao S, Powell RL, Lee AP, Longo ML, Dayton PA. Tailoring the size distribution of ultrasound contrast agents: Possible method for improving sensitivity in molecular imaging. Molecular Imaging. 2007; 6(6):384–392. [PubMed: 18053409]
25. Talu E, Hettiarachchi K, Powell RL, Lee AP, Dayton PA, Longo ML. Maintaining monodispersity in a microbubble population formed by flow-focusing. Langmuir. 2008; 24:1745–1749. [PubMed: 18205422]
26. Castro-Hernández E, van Hoeve W, Lohse D, Gordillo JM. Microbubble generation in a co-flow device operated in a new regime. Lab Chip. 2011; 11(12):2023–2029. [PubMed: 21431188]
27. Nisisako T, Torii T. Microfluidic large-scale integration on a chip for mass production of monodisperse droplets and particles. Lab Chip. 2008; 8:287–293. [PubMed: 18231668]
28. Kobayashi, Uemura K, Nakajima M. Formulation of monodisperse emulsions using submicron-channel arrays. Colloids and Surfaces A: Physicochem. Eng. Aspects. 2007; 296:285–289.
29. Teh S-Y, Lin R, Hung L-H, Lee AP. Droplet microfluidics. Lab Chip. 2008; 8:198–220. [PubMed: 18231657]
30. Anna SL, Mayer HC. Microscale tipstreaming in a microfluidic flow focusing device. Phys. Fluids. 2006; 18:121512.
31. Cubaud TC, Mason TG. Capillary threads and viscous droplets in square microchannels. Phys. Fluids. 2008; 20:053302.
32. Tan Y-C, Cristini V, Lee AP. Monodispersed microfluidic droplet generation by shear focusing microfluidic device. Sensors and Actuators B: Chemical. 2006; 114(1):350–356.
33. Garstecki P, Stone HA, Whitesides GM. Mechanism for flow-rate controlled breakup in confined geometries: A route to monodisperse emulsions. Phys. Rev. Lett. 2005; 94:164501. [PubMed: 15904231]
34. Xia Y, Whitesides G. Soft lithography. Annual Review of Materials Science. 1998; 28:153–184.
35. Hettiarachchi K, Zhang S, Feingold S, Dayton PA, Lee AP. Controllable microfluidic synthesis of multiphase drug-carrying lipospheres for site-targeted therapy. Biotechnol. Prog. 2009; 25(4):938–945. [PubMed: 19455647]
36. Martz TD, Sheeran PS, Bardin D, Lee AP, Dayton PA. Precision manufacture of perfluorocarbon droplets for acoustic droplet vaporization. Ultrasound Med. Biol. 2011
37. Arima K, Yamakado K, Kinbara H, Nakatsuka A, Takeda K, Sugimura Y. Percutaneous radiofrequency ablation with transarterial embolization is useful for treatment of stage 1 renal cell carcinoma with surgical risk: Results at 2-year mean follow up. International Journal of Urology. 2007; 14(7):585–590. [PubMed: 17645597]
38. Yamakado K, Anai H, Takaki H, Sakaguchi H, Tanaka T, Kichikawa K, Takeda K. Adrenal metastasis from hepatocellular carcinoma: Radiofrequency ablation combined with adrenal arterial chemoembolization in six patients. American Journal of Roentgenology. 2009; 192:W300–W305. [PubMed: 19457793]
39. Wu F, Wang Z-B, Chen W-Z, Zou J-Z, Bai J, Zhu H, Li K-Q, Jin C-B, Xie F-L, Su H-B. Advanced hepatocellular carcinoma: Treatment with high-intensity focused ultrasound ablation combined with transcatheter arterial embolization. Radiology. 2005; 235:659–667. [PubMed: 15858105]

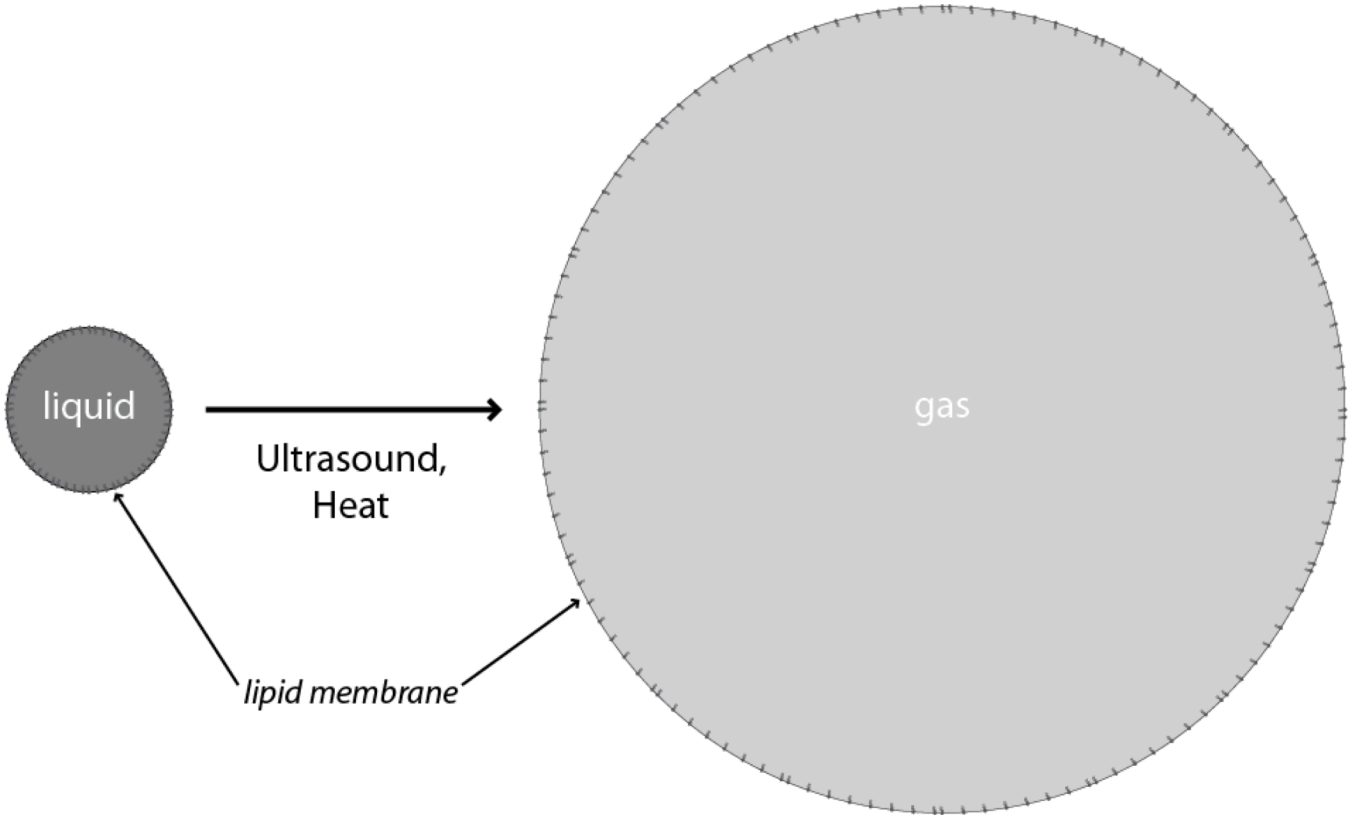

Fig. 1.

Schematic of the liquid-to-gas phase transition of a phase-change droplet. When presented with acoustic or thermal stimuli of a threshold amount, the volatile liquid core of the droplet rapidly vaporizes within the lipid shell. Expansion to a gas bubble enables the intentional occlusion of a target vessel *in vivo*. Other possible stimuli include light and mechanical pressure.

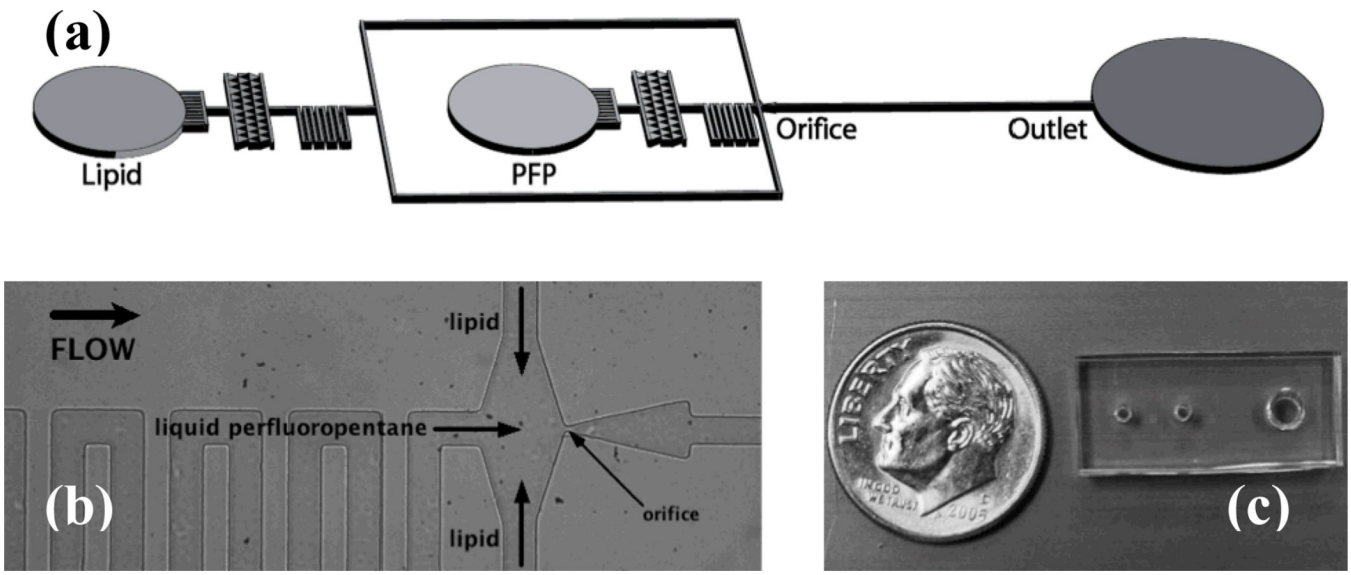

Fig. 2.

Geometry of the device for the generation of liquid perfluoropentane phase-change droplets. (a) Schematic view of the microfluidic flow-focusing device. All channels are rectangular with a height of 25 μm. (b) Image of the flow-focusing region. Lipid solution and liquid perfluoropentane distribution channels measure 38 μm in width and direct flows to a 7 μm orifice. Expanding nozzle geometry precedes a post-orifice channel 30 μm in width. (c) Overhead view of assembled PDMS device relative to a dime.

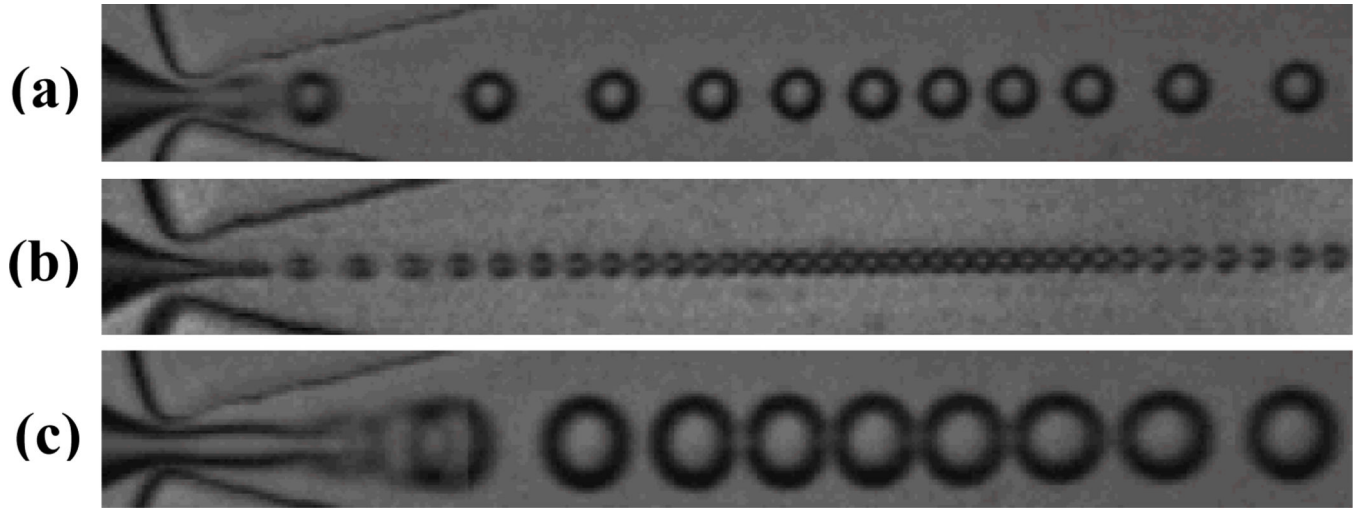

Fig. 3.

Representative images of three distinct droplet formation regimes. (a) Geometry-controlled. A series of overlaid images, successive in time, demonstrate the protrude-and-retract mechanism of the dispersed phase finger. (b) Dripping. Droplets break off from the tip of the dispersed phase finger at high rates due to “steady” Rayleigh capillary instability. (c) Jetting. A series of overlaid images, successive in time, demonstrate the break off of droplets due to “dynamic” Rayleigh capillary instability. Image height is 25 μm.

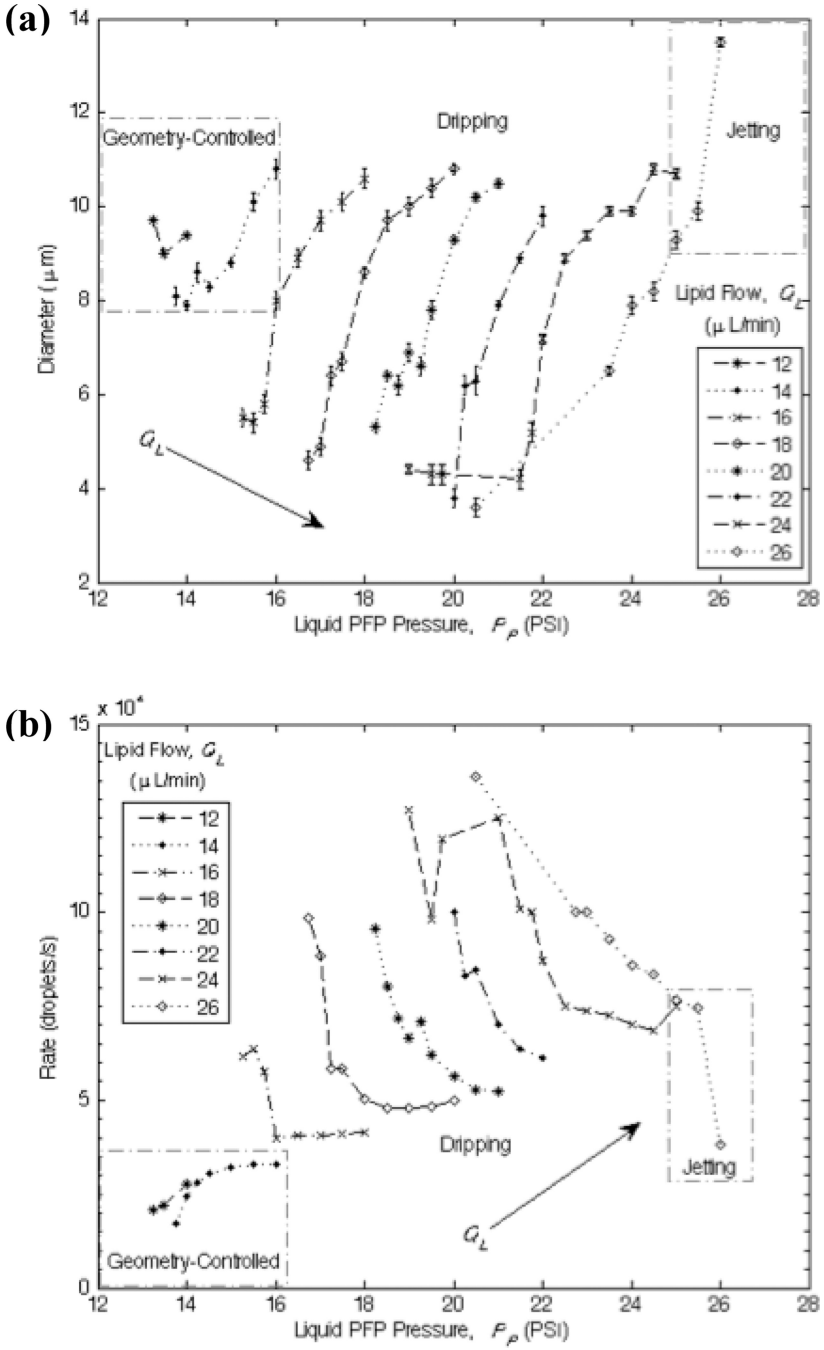

Fig. 4.

Diagrams of the production characteristics as determined by the flow parameters. Boxes distinguish geometry-controlled and jetting modes of droplet formation from dripping. (a) Droplet diameter D as a function of the lipid flow Q_L and the liquid perfluoropentane pressure P_P. (b) Generation frequency f_d as a function of Q_L and P_P.

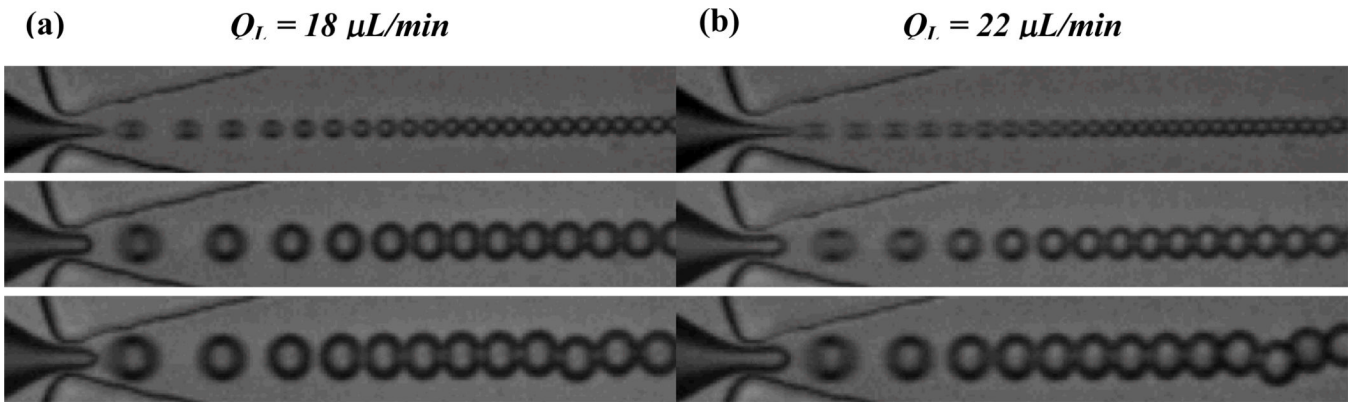

Fig. 5.

Sequence of images showing the effect of liquid perfluoropentane pressure for two lipid flows in the dripping regime. Droplet diameter decreases and generation frequency quickens as the dimensionless flow rate ratio $\varphi = Q_L/Q_P$ increases. (a) Q_L = 18 μL/min. Top to bottom: P_P = 17 PSI, φ = 55, D = 4.9 ± .2 μm, f_d = 8.82 × 10^4 Hz; P_P = 18 PSI, φ = 18, D = 8.6 ± .1 μm, f_d = 5.04 × 10^4 Hz; P_P = 19 PSI, φ = 9, D = 10.0 ± .2 μm, f_d = 4.80 × 10^4 Hz. (b) Q_L = 22 μL/min. Top to bottom: P_P = 20 PSI, φ = 128, D = 3.8 ± .2 μm, f_d = 1.00 × 10^5 Hz; P_P = 21 PSI, φ = 20, D = 7.9 ± .1 μm, f_d = 7.00 × 10^4 Hz; P_P = 22 PSI, φ = 12, D = 9.8 ± .2 μm, f_d = 6.12 × 10^4 Hz. Image height is 25 μm.

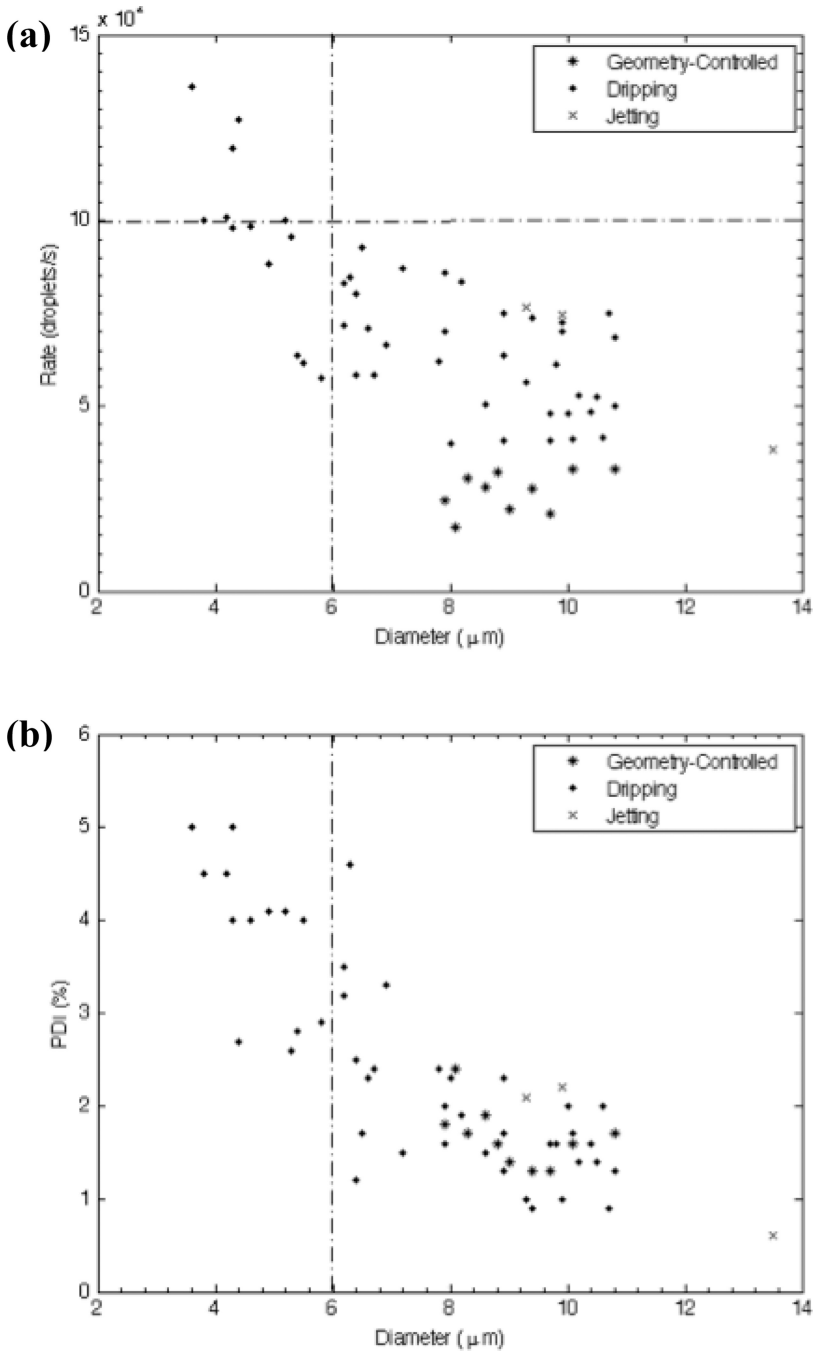

Fig. 6.

Plots relating generation frequency and polydispersity index to droplet size. The dripping regime enables droplet formation in the appropriate 3–6 μm range at high frequency and monodispersity. (a) Generation frequency f_d as a function of droplet diameter D. (b) Polydispersity index (PDI) as a function of D. All flow conditions generated droplets with PDI < 5%.

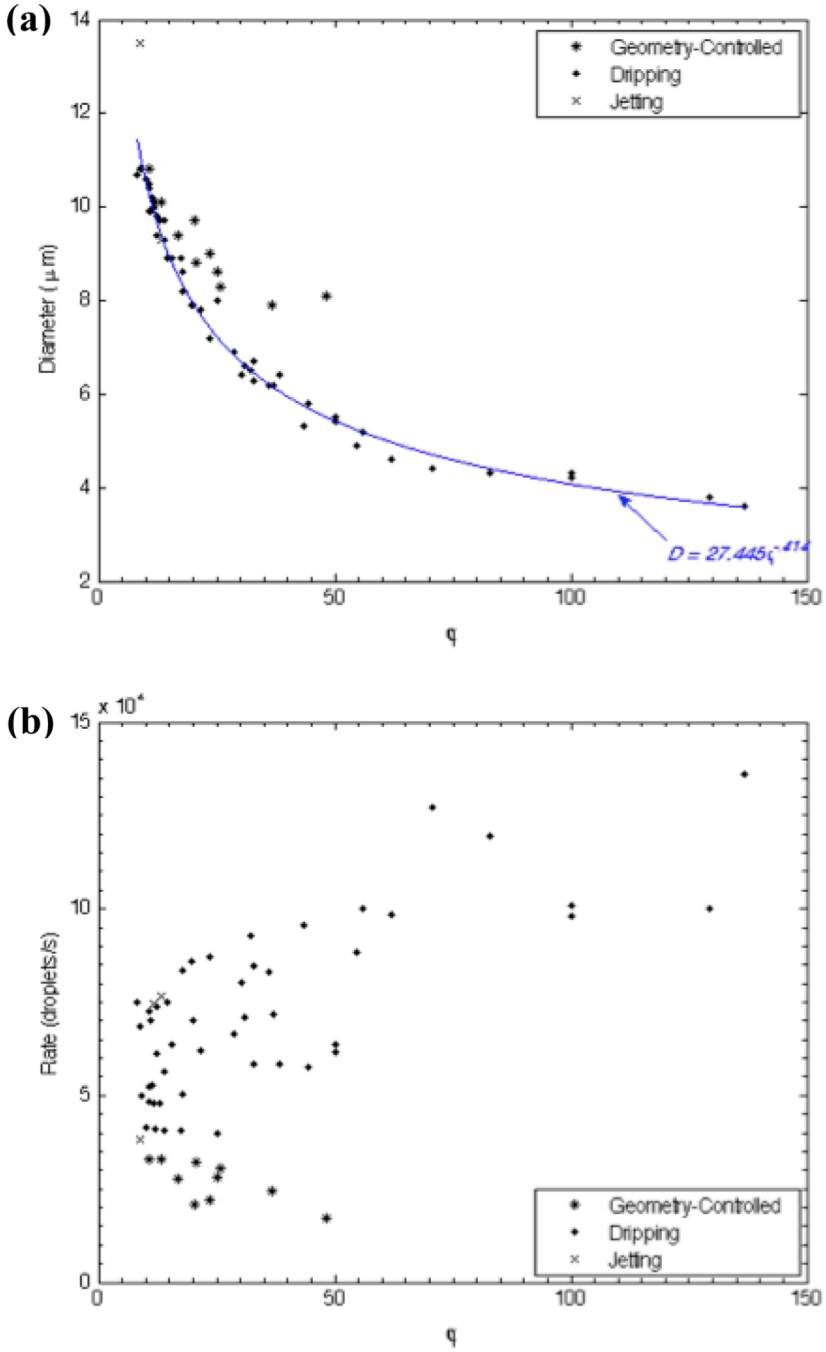

Fig. 7.

Diagrams of the production characteristics as determined by the ratio of the continuous lipid flow to the dispersed liquid perfluoropentane flow, $\varphi = Q_L/Q_P$. (a) Droplet diameter D as a function φ. For a given φ, droplet formation in geometry-controlled mode generates droplets of a larger size than in dripping. A power-series equation, valid in the dripping regime, emerges to predict droplet size based on the dimensionless flow rate ratio as $D = 27.445\varphi^{-.414}$ ($r^2 = .99$). (b) Generation frequency f_d as a function of φ. Increasing φ tends to slow f_d in geometry-controlled mode and quicken f_d in dripping.

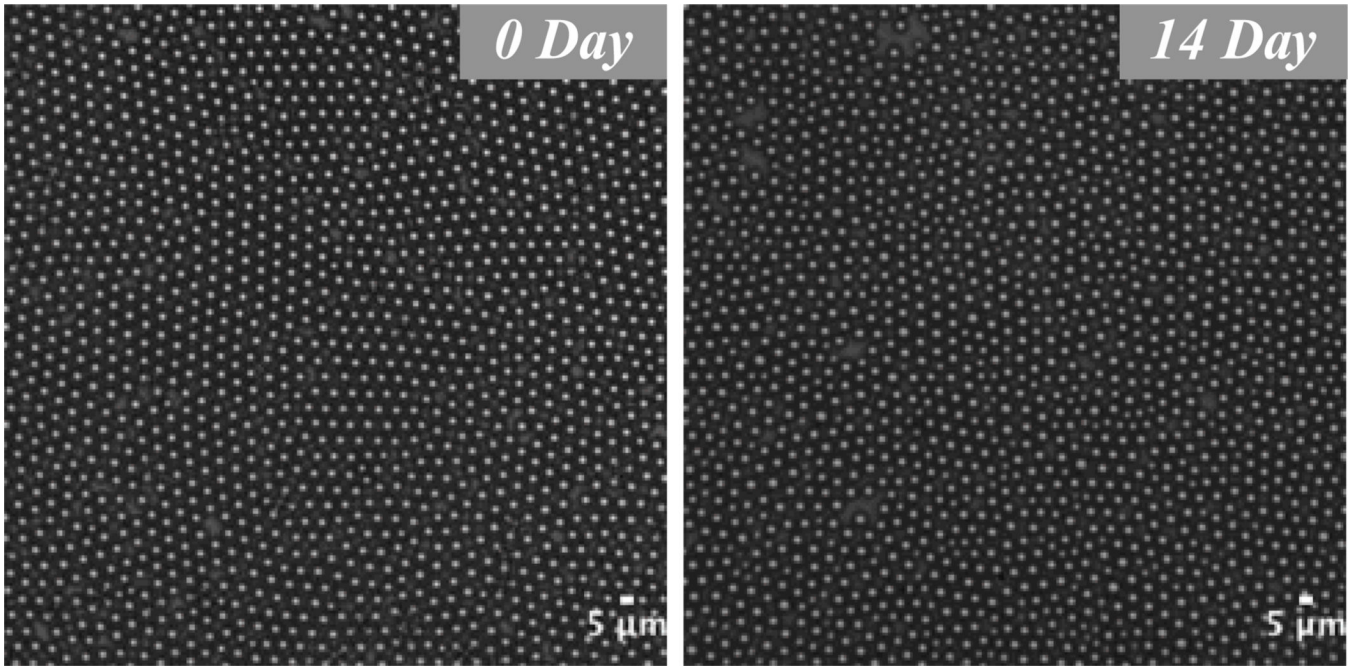

Fig. 8.

Images showing stability of a droplet population over a two-week time period. Droplets 4.5 µm in diameter drifted less than 4% in size over 14 days in a sealed glass vial at room temperature. Thus our phase-change droplets exhibited high stability in a true on-the-shelf setting. Scale bar represents 5 µm.

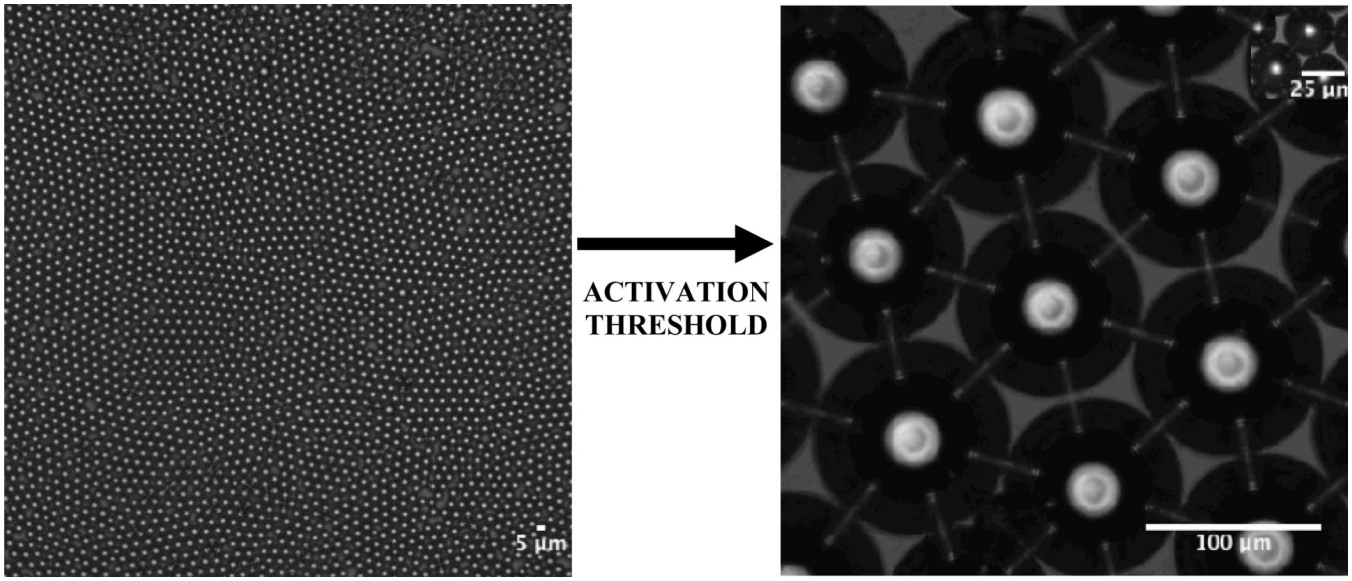

Fig. 9.

Thermal vaporization of a population of liquid perfluoropentane droplets after heating in a stirred water bath. Rapid droplet activation was observed at a water bath temperature of 88°C. Upon vaporization, 4.5 µm droplets initially transitioned into gas bubbles 106.7 µm in diameter. (inset) Occlusive bubbles with a resting diameter of 27.4 µm resulted following dissolution of extra gases.